ACS APPLIED MATERIALS & INTERFACES

Research Article

www.acsami.org

Oxidative Unzipping of Stacked Nitrogen-Doped Carbon Nanotube Cups

Haifeng Dong,‡ Yong Zhao,‡ Yifan Tang, Seth C. Burkert, and Alexander Star*

Department of Chemistry, University of Pittsburgh, Pittsburgh, Pennsylvania 15260, United States

Supporting Information

ABSTRACT: We demonstrate a facile synthesis of different nanostructures by oxidative unzipping of stacked nitrogen-doped carbon nanotube cups (NCNCs). Depending on the initial number of stacked-cup segments, this method can yield graphene nanosheets (GNSs) or hybrid nanostructures comprised of graphene nanoribbons partially unzipped from a central nanotube core. Due to the stacked-cup structure of as-synthesized NCNCs, preventing complete exposure of graphitic planes, the unzipping mechanism is hindered, resulting in incomplete unzipping; however, individual, separated NCNCs are completely unzipped, yielding individual nitrogen-doped GNSs. Graphene-based materials have been employed as electrocatalysts for many important chemical reactions, and it has been proposed that increasing the reactive edges results in more efficient electrocatalysis. In this paper, we apply these graphene conjugates as electrocatalysts for the oxygen reduction reaction (ORR) to determine how the increase in reactive edges affects the electrocatalytic activity. This investigation introduces a new method for the improvement of ORR electrocatalysts by using nitrogen dopants more effectively, allowing for enhanced ORR performance with lower overall nitrogen content. Additionally, the GNSs were functionalized with gold nanoparticles (GNPs), resulting in a GNS/GNP hybrid, which shows efficient surface-enhanced Raman scattering and expands the scope of its application in advanced device fabrication and biosensing.

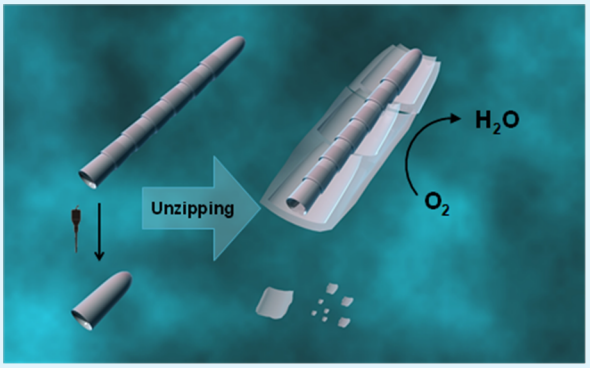

KEYWORDS: *nitrogen doped, carbon nanotubes, unzipping, graphene−carbon nanotube hybrid structure, optimized morphology*

INTRODUCTION

Carbon nanomaterials have attracted significant research interest, due to their unique electronic structure, including application to electrocatalysis,[1] microelectronics,[2] and bioimaging.[3,4] Doping of carbon nanostructures with nitrogen atoms alters the intrinsic properties of graphitic carbon materials due to interaction between the nitrogen lone-pair electrons and the graphene π-system,[5] producing tailored electronic characteristics and controllable surface and local chemical features. For instance, nitrogen-doped carbon nanotubes show high electrocatalytic activity toward the oxygen reduction reaction (ORR),[6,7] while nitrogen-doped graphene exhibits new tailored electronic properties for device applications.[8] Further manipulation of nitrogen-doped carbon nanotubes has resulted in nitrogen-doped graphene nanoribbons (GNRs) and nitrogen-doped graphene nanosheets (GNSs), both maintaining enhanced ORR activity.[9−11]

The ORR electrocatalytic activity of carbon nanomaterials is considered to be enhanced by increasing exposure of chemically active graphitic edges.[12,13] Recently, Li et al. developed a GNR−nanotube complex by exfoliating the outer graphene layer from double-walled CNTs,[14] enhancing ORR activity due to the combination of ORR-active GNRs with conductive CNT cores. A similar graphene support functionalized with carbon nanotubes hybrid structure synthesized from a hydrothermal process also showed advanced electrochemical performance.[15] These findings indicated hybrid nitrogen-doped structures as the optimized morphology for ORR electrocatalysis; however, both methods require a postsynthesis step of nitrogen-doping by NH_3 annealing, which adds to the synthetic complexity. Oxidative longitudinal unzipping of carbon nanotubes has been shown to effectively produce GNRs upon reaction with sulfuric acid (H_2SO_4) and potassium permanganate ($KMnO_4$).[16] This complete unzipping has been further demonstrated to produce nitrogen-doped GNRs from nitrogen-doped carbon nanotubes.[17] However, systematic investigation of morphological influence on the electrochemical properties of these nitrogen-doped hybrid nanomaterials remains undone.

Nitrogen-doped carbon nanotube cups (NCNCs) have been shown to be catalytically active toward ORR in their as-synthesized state; however, postsynthesis modification may further improve their activity. We demonstrate the synthesis of nitrogen-doped nanostructures by oxidative unzipping of NCNCs; the unique stacked cup-shaped segments allow for

Received: January 20, 2015
Accepted: May 6, 2015
Published: May 6, 2015

DOI: 10.1021/acsami.5b00447
ACS Appl. Mater. Interfaces 2015, 7, 10734−10741

modification of the unzipping mechanism, resulting in new nanostructures.[18,19] Different from the hollow, tubular, undoped CNTs, long-stacked NCNCs are more resistant to the unzipping process, resulting in a unique partially unzipped hybrid carbon nanostructure with nitrogen-doped GNRs connected through central tubular "cores". The extent of unzipping highly depends on the number of stacked cups in the NCNCs: upon ultrasonic separation of the stacked structure,[19,20] the obtained short-stacked and individual nanocups can be completely unzipped into graphene nanosheets (GNSs). GNSs have been previously synthesized by electrochemical exfoliation[21] or hydrothermal cutting[22] of graphene sheets. Although nitrogen doping of GNSs is typically performed by a postsynthesis step,[11] our approach provides a facile synthetic route to nitrogen-doped GNSs by direct unzipping of NCNCs.

Both partially and completely unzipped NCNCs may find promising applications in diverse fields due to their unique structural and chemical properties. The partially unzipped NCNCs exhibit excellent ORR electrocatalytic activity superior to as-synthesized NCNCs and their other derivatives; this observation provides a strong support for the GNR−carbon nanotube hybrid structure as the optimal morphology for electrocatalysis. Such enhancement results from the alteration of both nitrogen functionality and morphology of NCNCs by $H_2SO_4/KMnO_4$ oxidation. The nitrogen-doped GNRs formed on the unzipped part of the outer wall of the nanotubes make a more efficient ORR electrocatalyst, whereas the intact inner walls facilitate charge transport during electrocatalysis due to their retained electrical conductivity.

Surface-enhanced Raman scattering (SERS) has developed into an extremely useful technique for the detection of low concentration chemicals and biomolecules.[23] SERS is achieved when noble metal nanoparticles are in close proximity to Raman-active molecules, thus inducing dipole moments that enhance the inherent Raman signature. While free metal nanoparticles are able to induce SERS, it has been found that templating nanoparticles on a substrate, given optimized gaps between metal nanoparticles, allows for more sensitive and consistent SERS measurements, although most current fabrication techniques for SERS substrates are expensive and require complex instrumentation.[24,25] Moreover, graphene sheets have been explored in SERS applications as support for noble metal nanoparticles.[26,27] The doping of nitrogen atoms enhances the electronic structure of graphene for SERS[28] and promotes gold nanoparticle (GNP) binding affinity.[19,29] Here, the localized reactive sites of doped nitrogen atoms in the completely unzipped GNSs were employed to functionalize with GNPs to form a GNS/GNP hybrid composite, which exhibits efficient SERS detection of Rhodamine 6G, displaying potential application in chemical biosensing.

EXPERIMENTAL SECTION

Materials and Reagents. Pt/C 10% sample was received from Columbia Chemical Co. Nafion117 solution (5 wt %) and ferrocene were purchased from Sigma-Aldrich. H_2 and Ar gases were procured from Valley National Gases. Dimethylformamide (DMF), ethanol (EtOH), $KMnO_4$, xylenes, and H_2SO_4 were purchased from Fisher Scientific; acetonitrile and HNO_3 were purchased from EMD Millipore. All chemicals were used as received.

Preparation of Nitrogen-Doped Carbon Nanotube Cups (NCNCs). NCNCs were prepared following the published procedure.[19] Briefly, NCNCs were synthesized using chemical vapor deposition (CVD) in a Lindberg/Blue tube furnace. NCNCs were formed on a quartz substrate positioned in a quartz tube (1 in. diameter) inside the furnace. A mixture of liquid precursors consisting of 7.0 wt % of acetonitrile, 0.75 wt % of ferrocene, and 92.25 wt % of xylenes was passed through the quartz tube at a rate of 1 mL/min with carrier gases of Ar at 126.8 sccm and H_2 at 37.5 sccm at 800 °C for 1 h. The CVD furnace was then cooled down to room temperature under an Ar atmosphere for 1 h. NCNCs product grown on the quartz substrate was then scraped off and collected using a double-sided razor blade.

Chemical Oxidation and Unzipping of NCNCs. Approximately 5 mg of as-synthesized NCNCs was first transferred to a 3:1 mixture of 95−98% sulfuric acid and 68% nitric acid (20 mL). The mixture was then sonicated in a Branson 1510 bath sonicator at a power of 80 W for 4 h at room temperature. Subsequently, 80 mL of water was added and this material was collected by filtration using a polytetrafluoroethylene (PTFE) membrane filter (200 nm pore size), washed thoroughly with water, and dried overnight under vacuum at 60 °C. The resulting o-NCNCs (oxidized NCNCs) were directly unzipped to obtain u-NCNCs (unzipped NCNCs) using a previously reported $H_2SO_4/KMnO_4$ oxidative treatment.[30] Alternatively, o-NCNCs were processed into separated NCNCs (s-NCNCs) through probe-tip sonication. Briefly, the o-NCNCs aqueous solution (0.1 mg/mL) was sonicated at a 500 W probe-tip sonicator (Fisher Scientific FB505) for a total of 8 h (30 s on and off) in ice bath.

For typical unzipping procedure of o-NCNCs, 2 mg of o-NCNCs was added to 2 mL of 98% sulfuric acid and the mixture incubated for 18 h. Subsequently, 10 mg of $KMnO_4$ was gradually added to the solution while the temperature was kept at 65 °C for 2 h. The reaction was then quenched by the addition of 10 mL of ice water containing 125 μL of 30% H_2O_2 solution. The solution was filtrated through a PTFE membrane (0.2-μm pore size), and the solid was washed with 5% HCl solution three times (20 mL each time) and water three times (20 mL each time). The final product was dried in vacuum to obtain u-NCNCs. For unzipping s-NCNCs (separated NCNCs), the same procedure was followed.

Material Characterization. Low-resolution TEM images were obtained with a Philips/FEI Morgagni at an accelerating voltage of 80 kV. High-resolution TEM images were taken using a JEOL 2100F microscope with an accelerating voltage of 200 kV. TEM samples were prepared by drop-casting the nanomaterial suspension in DMF or EtOH on a lacey carbon TEM grid (Pacific Grid-Tech) for low-resolution TEM imaging or on a C-FLAT holey TEM grid (Electron Microscopy Sciences) for high-resolution TEM imaging. SEM images were performed with a Phillips XL30 FEG microscope equipped using an EDAX assembly.

XPS spectra were collected on Thermo Scientific K-Alpha X-ray photoelectron spectrometer using monochromated Kα X-rays (1486.6 eV). The sample spot size was 400 μm, with a pass energy of 200 eV for the survey scans and 50 eV for high resolution. Charge compensation was provided by a low-energy electron source and Ar^+ ions. XPS samples were prepared by briefly sonicating the NCNCs in ethanol, drop-casting them onto an aluminum substrate, and allowing the solvent to evaporate completely. The spectra were fitted after background subtraction of a Shirley-type baseline. Peak shapes were optimized by using a Gaussian:Lorentzian ratio of 80:20. The fwhm was set within the range 1.5−3.0. Raman spectra were collected on a Reinshaw inVia Raman microscope with an excitation wavelength of 633 nm with a scan wavelength range from 1000 to 2000 cm^{-1} at 10% laser power (maximum 17 mW) with 15 s exposure time. Samples were drop-cast on a quartz slide and dried prior to characterization.

Electrochemical Measurements. All electrochemical measurements including cyclic voltammetry (CV), rotating ring disc electrochemistry (RRDE), linear sweep voltammetry (LSV), and chronoamperometry measurements were performed using a CHI 7042 Bipotentiostat (CH Instruments, Austin, TX). A Pt wire electrode (CHI 115) and a Ag/AgCl (CHI 111, 1 M KCl) electrode were used as the counter and reference electrode, respectively. All potentials are reported with respect to Ag/AgCl. The electrodes were purchased from CH Instruments, Austin, TX. The RRDE was purchased from Pine Instrument Co. (AFE7R9GCPT; reported collection efficiency N = 0.37) containing a glassy carbon (GC) disk and Pt ring electrode.

DOI: 10.1021/acsami.5b00447
ACS Appl. Mater. Interfaces 2015, 7, 10734−10741

Scheme 1. (A) Schematic Illustration of Unzipping Nitrogen-Doped Carbon Nanotube Cups (NCNCs)[a] and the Unzipping Process on the Surface of (B) o-NCNCs and (C) s-NCNCs[b]

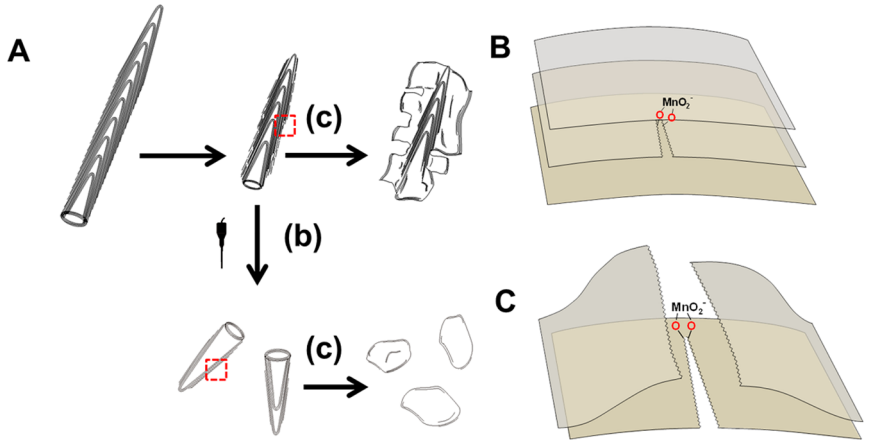

[a]Reagents and conditions: (a) H_2SO_4/HNO_3 (3:1 v/v), bath sonication (4 h); (b) water, tip sonication (8 h); (c) H_2SO_4 (18 h), $KMnO_4$ (65 °C, 2 h). [b]The red dashed boxes on the o-NCNCs and s-NCNCs indicate the location of the unzipping mechanisms illustrated in B and C.

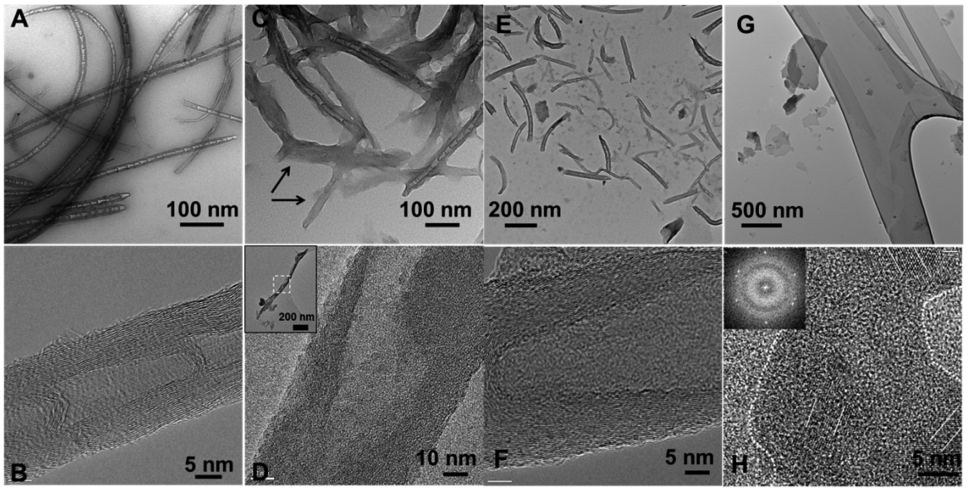

Figure 1. Structural characterization of various carbon nanomaterials. Transmission electron microscopy (TEM) images of (A) oxidized NCNCs (o-NCNCs); (C) partially unzipped NCNCs (u-NCNCs), where arrows indicate the completely unzipped part; (E) separated NCNCs (s-NCNCs) after probe-tip sonication of the material in part A; and (G) graphene nanosheets (GNSs) after unzipping of the material in part E. High-resolution TEM images of (B) o-NCNCs, (D) u-NCNCs, (F) s-NCNCs, and (H) GNSs. The inset in part D is the entire u-NCNCs from which the HRTEM image was obtained. The inset in H is the fast Fourier transform (FFT) of GNSs, where dotted white lines show the outline of the GNS and solid white lines highlight several graphitic lattices.

The RRDE experiments were performed on a MSR Electrode Rotator. A GC electrode (CHI 104, GC area 0.0707 cm^2, total area 0.196 cm^2) or rotating ring-disk electrode (GC disk area 0.2475 cm^2) was carefully polished with γ-alumina powder (0.05 μm, CH Instruments) to obtain a mirror finish, rinsed and sonicated with double distilled water to remove any alumina residues, and finally dried under N_2.

Catalyst ink was made by dissolving 1 mg of NCNCs or Pt/C sample in a solvent mixture of 992 μL of ethanol and 8 μL of 5% Nafion by sonication for at least 30 min to give a concentration of 1 mg/mL NCNCs and 0.04% Nafion. A 20 μL portion of catalyst ink was then drop-cast on the GC electrode or the GC part for RRDE and allowed to air-dry. For RRDE voltammetry, LSV was performed using modified RRDE in O_2-saturated 0.1 M KOH solution at a scan rate of 0.05 V/s and rotating speed of 1400 rpm (rpm) while the Pt ring was polarized at 0.5 V for oxidizing H_2O_2. Chronoamperometric response was tested by holding the electrode at −0.3 V for 8 h. The tests were repeated at least three times to confirm the reproducibility of the process. The collection efficiency of RRDE was confirmed by testing in 10 mM $K_3Fe(CN)_6$ solution with 0.5 M KNO_3 as the supporting electrolyte.

GNP Functionalization and SERS Characterization. About 5 mL of 0.005 mg/mL GNSs unzipped from separated NCNCs was added with 250 μL of 1 mg/mL $HAuCl_4$ solution, and the mixture stirred on a hot plate at 70 °C for 20 min. Then 150 μL of 1 wt % trisodium citrate solution was added dropwise and the reaction was stirred for another 2 h. The GNP-functionalized GNSs were collected by centrifugation at 3400 rpm and resuspended in ∼1 mL of water. Rhodamine 6G (R6G) or 123 (Rh123) with different low concentrations was added into the GNS solution, and 20 μL was drop-cast on a glass slide for Raman spectroscopy.

RESULTS AND DISCUSSION

NCNCs were synthesized using a floating catalyst CVD method as outlined in our previous reports.[19,20,31,32] The oxidation process was carried out by bath sonication of as-synthesized NCNCs in a mixture of H_2SO_4/HNO_3 (3:1 v/v) for 4 h. The oxidized NCNCs, termed herein as o-NCNCs, were then treated with $H_2SO_4/KMnO_4$, resulting in partially unzipped NCNCs (u-NCNCs). Alternatively, o-NCNCs were

DOI: 10.1021/acsami.5b00447
ACS Appl. Mater. Interfaces 2015, 7, 10734−10741

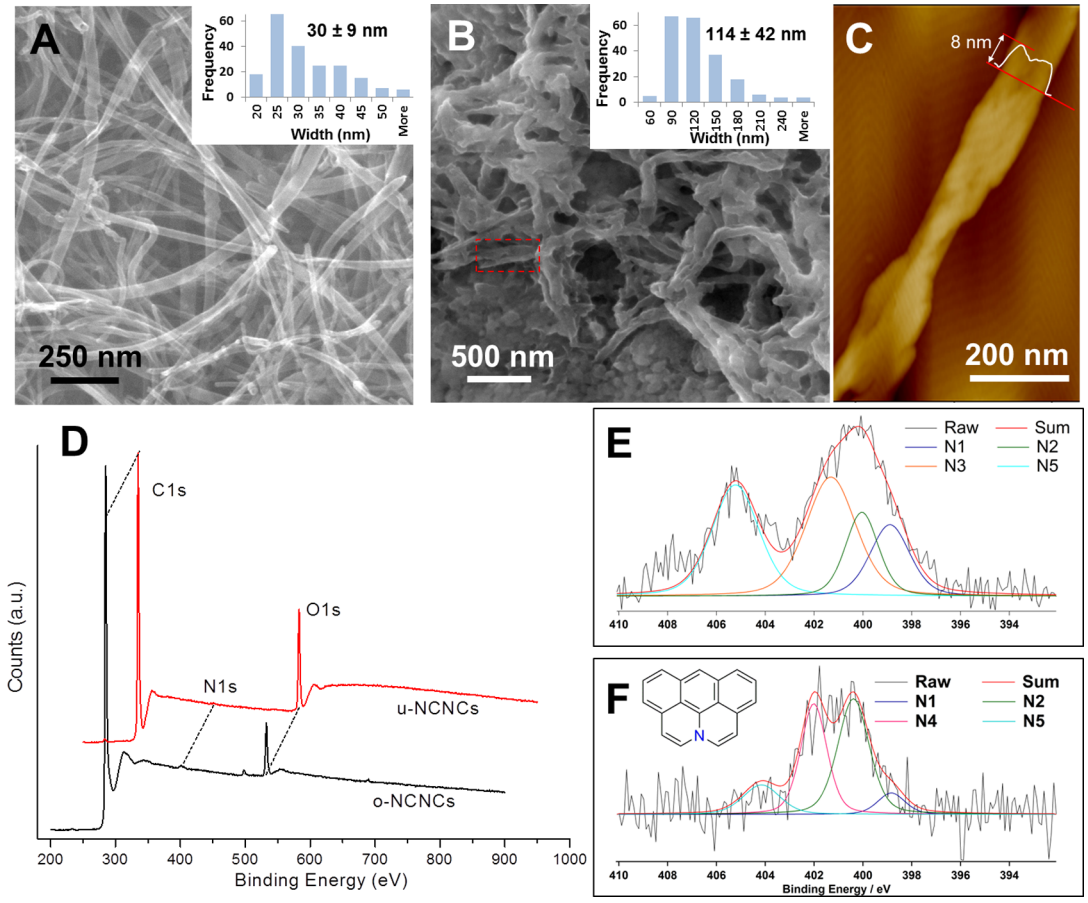

Figure 2. Surface morphology and compositional characterization. Scanning electron microscopy (SEM) images of (A) o-NCNCs and (B) u-NCNCs. The insets show the width distribution of corresponding materials. (C) Atomic force microscopy (AFM) of u-NCNCs. (D) X-ray photoelectron spectroscopy (XPS) survey scan of u-NCNCs (red) and o-NCNCs (black). (E, F) XPS N 1s spectra of o-NCNCs and u-NCNCs. The inset in part F shows the chemical structure of a valley-N.

separated by high-intensity probe-tip sonication to yield separated NCNCs (s-NCNCs) consisting of many short-stacked and individual nanocups,[19,20] which were then unzipped by the same $H_2SO_4/KMnO_4$ treatment, forming nitrogen-doped GNSs (Scheme 1).

Figure 1 shows transmission electron microscopy (TEM) images of the corresponding materials. After the oxidation process, o-NCNCs largely maintained the morphology of stacked cup-shaped compartments of the initial material with diameters of 30−50 nm and lengths of 1−2 μm (Figure 1A). High-resolution TEM (HRTEM) images in Figure 1B exhibit the well-defined multiwalled graphitic lattices that are curved at the tip of each stacked cup and extend to the surface of the sidewalls, as illustrated in Scheme 1A. Unlike unzipping undoped multiwalled carbon nanotubes (MWCNTs), which produces free-standing graphene nanoribbons,[16] $H_2SO_4/KMnO_4$ treatment of o-NCNCs afforded a graphene/nanotube hybrid structure, in which the outer graphitic layers of o-NCNCs were partially exfoliated but still attached to the inner tubular cores. As shown in Figure 1C, the sidewalls of NCNCs became distorted and indistinct after unzipping as carbonaceous sheets were formed, spreading around the nanotubes. In most cases, the inner cup-shaped tubular cores are still present, although the tubular structures were occasionally completely destroyed, leaving only GNRs. Figure 1D shows a magnified image of the partially exfoliated sheets from a NCNC fiber undergoing the unzipping process. Graphitic lattices were still observed at the edge of the opened sheet, indicating that the unzipping process can penetrate several layers and form few-layer graphene sheets. Such a partial unzipping phenomenon was also observed in a recent study by Cruz-Silva et al. on nitrogen-doped CNTs with diameters less than 50 nm,[17] in contrast to the complete unzipping of undoped MWCNTs under the same condition.[16] We propose that the different unzipping behaviors may be attributed to the different morphologies of the two carbon nanomaterials. For MWCNTs, the graphitic walls are parallel to the tube axis, leaving a hollow tubular structure. According to the proposed unzipping mechanism,[16,30] the unzipping starts from the addition of manganese ester to C=C bonds on the exposed graphitic planes and propagates along the adjacent alkene groups on the same plane. Due to the unique stacked-cup structure of NCNCs, the tip of an individual cup is shielded from the external environment due to its insertion into the preceding cup, preventing the exposure of continuous graphitic planes on the outer surface of NCNCs. As a result, unzipping the surface of NCNCs requires simultaneous breaking of multiple graphitic planes from different layers and thus is more energetically hindered (Scheme 1B).

To further investigate the unzipping mechanism, the stacked graphitic nanocups were first isolated out of their stacked structure through probe-tip sonication prior to the unzipping procedure.[19,20] After the ultrasonic separation, most of the NCNC segments were shortened to about 200 nm, consisting

DOI: 10.1021/acsami.5b00447
ACS Appl. Mater. Interfaces 2015, 7, 10734−10741

of either individual nanocups or several stacked-cup segments (Figure 1E). The separation did not alter their graphitic nature (Figure 1F). Instead, along with the separation of inserted cups, the previously inaccessible graphitic tips of NCNCs have been exposed and their subsequent complete unzipping is unhindered. After the same treatment procedure with $H_2SO_4/KMnO_4$, the cup-shaped structures were completely unzipped and transformed into flakelike GNSs (Figure 1G). The unzipping appears to take place longitudinally along the cup axis (Figure S1A, Supporting Information), in accordance with previous studies.[16,17] The sizes of the nanosheets appear to be correlated to the initial length of the s-NCNCs, which ranges from apparent 5−10 nm graphene quantum dots to larger flakes hundreds of nanometers in size. HRTEM (Figure 1H) shows the graphitic nature of the unzipped GNSs, with distinct carbon atoms forming six-membered rings. The small-sized GNSs mostly exist as single-layer graphene according to the FFT pattern, while larger flakes tend to have several layers of graphene sheets (Figure S1B, Supporting Information). The complete unzipping of s-NCNCs indicates that $H_2SO_4/KMnO_4$ oxidation is more favorable on fully exposed graphene surfaces, which is achieved when the stacked nanocups are separated (Scheme 1C).

The morphology change after the partial unzipping process on o-NCNCs was further revealed by scanning electron microscopy (SEM). NCNCs after acid oxidation still preserved a smooth surface with no apparent damage (Figure 2A). The unzipping process opened the outer surface, forming graphitic nanoribbons wrapped around the inner tubular structure, leaving the surfaces of the NCNC/graphene hybrid structure wrinkled and distorted (Figure 2B). Some of the NCNCs are still undergoing unzipping with graphitic sheets being unfolded outside (dashed blocks, Figure 2B). The atomic force microscopy (AFM) image further depicts the structure of a partially unzipped NCNC fiber (Figure 2C). The fiber has a rough surface and uneven width from 80 to 160 nm, indicating that the graphitic layers are unzipped from different sections of the nanotube. The height profile shows a concaved shape at the unzipped section, where the outer graphitic layers are opened from the middle and unfolded at both sides of the fiber with a thickness of 8 nm. AFM of GNSs shows a similar height profile between different sheets with a height of ∼1 nm corresponding to single- or double-layer graphene sheets (Figure S2, Supporting Information). The unzipping process increases the average width of NCNCs from 30 to 114 nm according to measurements from SEM images (Figure 2A,B inset). As indicated through the height profile of u-NCNCs and the increase in the average width of NCNCs from o-NCNCs to u-NCNCs, unzipping NCNCs exposes the inner graphitic layers that were previously inaccessible in addition to revealing the inside wall of the outer graphitic layer, which would effectively increase the surface area of the material and its subsequent catalytic activity.

Compared to the o-NCNCs, the X-ray photoelectron spectroscopy (XPS) analysis (Figure 2D) shows that the unzipping process by $H_2SO_4/KMnO_4$ oxidation causes an increase in the overall oxygen content of u-NCNCs, due to formation of oxygen groups, primarily in the form of carbonyl and carboxylic groups (Figure S3, Supporting Information), and a decrease in the nitrogen content, possibly resulting from the generation of gaseous nitrogen species.[33] Both H_2SO_4/HNO_3 and $H_2SO_4/KMnO_4$ oxidation processes lead to increasing amounts of defects on the graphitic structures, as confirmed by the increased D/G ratio from Raman spectra (Figure S4, Supporting Information). The high-resolution N 1s scans show changes of the nitrogen functionalities as a result of the unzipping process (Figure 2E,F). Before unzipping, the spectrum of o-NCNCs can be deconvoluted into four peaks at 398.7 eV (N1), 399.8−400.3 eV (N2), 401−401.6 eV (N3), and 405 eV (N5), which can be assigned to pyridinic, pyrrolic/amine, graphitic, and oxidized nitrogen species, respectively.[33] After unzipping, oxidized nitrogen is mostly removed, as shown by the decrease in the N5 peak in the u-NCNCs N 1s XPS scan, which is likely removed under the strong oxidation conditions. The peak of pyrrolic/amine groups increased, which would be formed through the unzipping process that converts nitrogen previously contained within the graphitic lattice to edge nitrogen functionalities.[28] A new peak appears at 402.3 eV (N4), which can be assigned to the nitrogen at the "valley" site between two benzene rings (inset, Figure 2F). According to the proposed mechanism by Cruz-Silva et al.,[17] the valley-N is likely transformed from graphitic N during oxidation due to the breaking of peripheral carbon−carbon bonds.

The XPS analysis on s-NCNCs and the completely unzipped GNSs also shows a decrease of nitrogen concentrations after the unzipping process (Figure S5A, Supporting Information). The high-resolution N 1s spectrum of s-NCNCs shows primarily graphitic and pyrrolic/amine nitrogen functionalities (Figure S5B, Supporting Information). The $KMnO_4$ oxidative unzipping process on the s-NCNCs caused a decrease in overall nitrogen content of the GNSs. The high-resolution N 1s spectrum of GNSs shows that the nitrogen exists primarily as pyrrolic/amine nitrogen, similar to the case of unzipping o-NCNCs (Figure S5C, Supporting Information). Survey XPS data containing atomic percentages and high-resolution N 1s XPS data containing percentages of nitrogen functionalities are summarized in Tables S1 and S2 (Supporting Information), respectively.

Because the existence of nitrogen alters the local electronic structure and makes the peripheral carbon networks more vulnerable to MnO_4^- oxidation,[17] we infer that the unzipping of s-NCNCs is preferentially induced by the nitrogen defective edges. This is evidenced by the decrease of nitrogen content from the XPS results after unzipping. Due to the small initial size of s-NCNCs and the increasing amount of defects created by probe-tip sonication (Figure S3, Supporting Information), the unzipping may take place from multiple nitrogen-functionalized defective sites on s-NCNCs and propagate simultaneously, which more easily cuts the graphitic planes into many GNS-sized fragments.

Nitrogen-doped carbon nanomaterials have been shown to have excellent potential as ORR electrocatalysts, and as such we analyzed our GNR/nanotube hybrid materials to determine how their difference in structure and nitrogen doping affects their electrocatalytic activity toward the ORR. RRDE was performed in order to determine the half-wave potential of materials as well as the electron transfer number for ORR as determined by eq 1, where I_D is the disc current, I_R is the ring current, and the N is the collection efficiency (0.37). Cyclic voltammetry was also performed and is included in Figure S6 (Supporting Information).

$$n = \frac{4I_D}{I_D + \frac{I_R}{N}} \quad (1)$$

DOI: 10.1021/acsami.5b00447
ACS Appl. Mater. Interfaces 2015, 7, 10734−10741

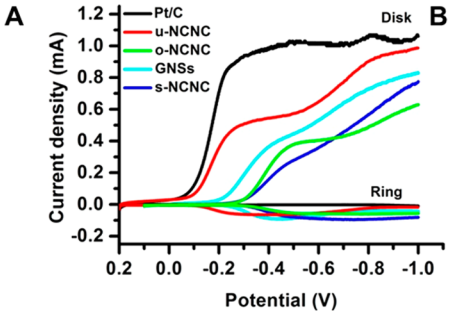

B

Material	*a*	*b*
Pt/C	−0.173	4.0
u-NCNC	−0.179	3.1
o-NCNC	−0.383	2.9
GNSs	−0.317	2.6
s-NCNC	−0.388	2.3

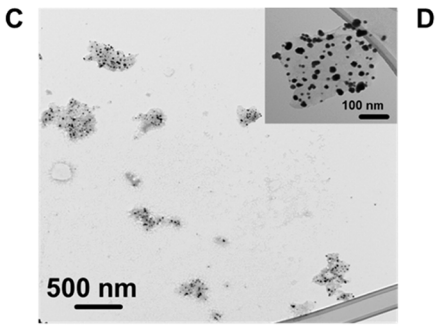

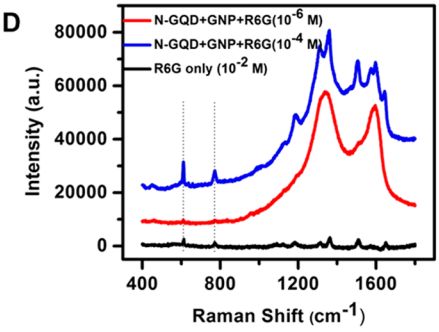

Figure 3. Applications of unzipped NCNCs: (A) RRDE voltammograms of commercial 10% Pt/C (black), u-NCNCs (red), o-NCNCs (green), GNSs (cyan), and s-NCNCs (blue) catalysts in O_2-saturated 0.1 M KOH with a rotating speed of 1400 rpm; (B) tabulated electrochemical values of all materials for (*a*) half-wave potential (V) and (*b*) electron transfer number (*n*); (C) TEM image of graphene nanosheets obtained from unzipping s-NCNCs after functionalization with gold nanoparticles (GNPs), with the inset showing a magnified TEM image of GNP-functionalized GNS; and (D) SERS of GNP-functionalized GNSs sensing probe molecules of Rhodamine 6G.

Figure 3A shows the RRDE scans for all synthesized materials. Electrodes fabricated from u-NCNCs showed the best ORR performance with a half-wave potential of −0.179 V, which is comparable to that of commercial Pt/C at −0.173 V. u-NCNCs show a drastic improvement in ORR performance over o-NCNCs, with a half-wave potential of −0.383 V despite a decrease in overall nitrogen content. This improvement must therefore be attributed to the increase in valley-N edge functionalities, which have been shown to be more active toward ORR, providing a more efficient use of doped nitrogen atoms.[33,34] The electron transfer number of u-NCNCs was found to be 3.1, which is an improvement upon not only that of o-NCNCs (2.9) but also pristine NCNCs, which have a calculated electron transfer number of 2.6.[32] The synthesized u-NCNCs also improve upon the previously reported graphene/nanotube composite materials by improving the half-wave potential without necessitating an increase in the overall nitrogen content of the material, providing a new avenue for ORR electrocatalyst development.[15] Upon separation of o-NCNCs to s-NCNCs, a decrease in half-wave potential, maximum current, and electron transfer number is observed. The diminished activity of s-NCNCs can be attributed to their shortened length, which is comparable to their diameter, resulting in a lower aspect ratio and denser packing of the s-NCNCs. This denser packing would result in an increased number of contact points between individual cups, yielding a higher resistance than that of o-NCNCs and u-NCNCs. Unzipping s-NCNCs to GNSs shows an increase in ORR activity, similar to that between o-NCNCs and u-NCNCs, indicating that unzipping NCNCs facilitates the formation of active edges on the outer graphene sheets, thus improving the ORR performance of NCNC-based materials. Although GNSs should have the highest surface area of all synthesized materials, they do not show the most improved electrochemical performance. This indicates the necessity of a central carbon nanotube core for the most effective ORR electrocatalyst. All electrochemical data is summarized in Figure 3B.

Platinum, the most common ORR electrocatalyst, has many performance issues, as surface deactivation occurs in response to the methanol crossover effect and CO poisoning, in addition to a consistent decrease in ORR activity on extended time scales. The activity of the u-NCNCs was tested for these concerns, as shown in Figure S7 (Supporting Information), and in all cases, u-NCNCs outperformed a commercial Pt/C electrocatalyst, with u-NCNCs showing no loss in ORR activity in response to the addition of 3 M methanol, 30% better activity over Pt/C upon exposure to CO gas, and a long-term stability of 90% of the initial current as compared to only 80% for the Pt/C after 7 h.

Furthermore, the nitrogen-doped GNSs may have additional interesting applications as surface-enhanced Raman substrates. Facilitated by the rich nitrogen functionalities, the GNSs can be evenly decorated with gold nanoparticles (GNPs). Figure 3C shows the TEM image of the graphene nanosheets evenly functionalized with GNPs with diameters of about 20 nm presumably anchored on the local nitrogen functionalities. The island distribution of GNPs on graphene nanosheets causes SERS on the graphene substrate (Figure S8A, Supporting Information), which can be used for highly sensitive SERS detection of biomolecules. To illustrate this application, we incubated the GNP/graphene nanosheets with the Raman probe molecule R6G at low concentrations and drop-cast 20 μL from each sample on glass slides for Raman spectra. Figure 3D shows that without the SERS substrate, pure R6G solution drop-cast on a glass slide incurred very weak Raman signals, even at high concentration of 10^{-2} M. However, significantly enhanced signals were observed in the presence of GNP/graphene nanosheets at 10^{-4} M of R6G, which corresponds to

DOI: 10.1021/acsami.5b00447
ACS Appl. Mater. Interfaces 2015, 7, 10734−10741

enhancement of more than 100 times. The detection limit can be as low as 10^{-6} M under our current conditions; the signals at even lower concentration tend to be overshadowed by those of the graphene nanosheets. Similar SERS effect is observed for Rh123 (Figure S8B, Supporting Information). We speculate that the SERS signals arise from the optimal diameters and interparticle distances of GNPs that provide coupled surface plasmon resonance (SPR) and significantly enhance the local electromagnetic field.[35] The enhanced SERS sensitivity, combined with suitable functionalization chemistry of the GNS/GNP composite, can lead to new classes of novel nanomaterials for drug delivery and in vivo SERS spectrum imaging.

CONCLUSION

Previous reports attempting to improve the ORR activity of nitrogen-doped carbon nanomaterials have relied on an increase of the overall nitrogen content. The findings in this report introduce an additional way to improve the ORR that relies on a more effective use of inherent nitrogen functionalities, through the creation of edge functionalities, as opposed to an increase in overall content. The increase in ORR performance with an overall decrease in nitrogen content allows for future advancement in ORR electrocatalysts without necessitating increased nitrogen content, which is difficult to achieve through standard synthesis methods. The large surface area of GNSs affords them as a potential substrate for sensing applications, and further decoration with GNPs increases their inherent Raman signal. Interaction of biomolecules with this SERS substrate allows for enhancement of their Raman peaks for a detection limit 100 times lower than can be achieved with unfunctionalized GNSs.

ASSOCIATED CONTENT

Supporting Information

TEM and HRTEM images of GNS, AFM of GNSs, C 1s high-resolution XPS of o-NCNCs and u-NCNCs, Raman spectra of all synthesized materials, survey XPS and N 1s high-resolution XPS of s-NCNCs and GNSs, table of atomic content determined by XPS, table of nitrogen functionality percentages determined by N 1s high-resolution XPS, cyclic voltammetry of all synthesized materials, cyclic voltammetry illustrating the methanol crossover effect, chronoamperometric response of CO poisoning, long-term stability of u-NCNCs, Raman spectra of GNP functionalized GNS, and SERS enhancement of Rh123. The Supporting Information is available free of charge on the ACS Publications website at DOI: 10.1021/acsami.5b00447.

AUTHOR INFORMATION

Corresponding Author

*E-mail: astar@pitt.edu.

Author Contributions

‡These authors contributed equally.

Notes

The authors declare no competing financial interest.

ACKNOWLEDGMENTS

This work is supported by NIEHS Award R01ES019304 and NSF CAREER Award No. 0954345. The authors thank the Nanoscale Fabrication and Characterization Facility and the Department of Biology of the University of Pittsburgh for provision of access to instruments. Y.Z. is thanksful for the support from a Bayer MaterialScience Fellowship.

REFERENCES

(1) Yu, D.; Zhang, Q.; Dai, L. Highly Efficient Metal-Free Growth of Nitrogen-Doped Single-Walled Carbon Nanotubes on Plasma-Etched Substrates for Oxygen Reduction. *J. Am. Chem. Soc.* **2010**, *132*, 15127−15129.

(2) Han, W.-Q.; Kohler-Redlich, P.; Seeger, T.; Ernst, F.; Rühle, M.; Grobert, N.; Hsu, W.-K.; Chang, B.-H.; Zhu, Y.-Q.; Kroto, H. W. Aligned CN_x Nanotubes by Pyrolysis of Ferrocene/C_{60} under NH_3 Atmosphere. *Appl. Phys. Lett.* **2000**, *77*, 1807.

(3) Baker, S. N.; Baker, G. A. Luminescent Carbon Nanodots: Emerging Nanolights. *Angew. Chem., Int. Ed.* **2010**, *49*, 6726−6744.

(4) Wong, N.; Kam, S.; Connell, M.; Wisodm, J. A.; Dai, H. J. Carbon Nanotubes as Multifunctional Biological Transporters and Near-Infrared Agents for Selective Cancer Cell Destruction. *Proc. Natl. Acad. Sci. U. S. A.* **2005**, *102*, 11600−11605.

(5) Wang, X.; Li, X.; Zhang, L.; Yoon, Y.; Weber, P. K.; Wang, H.; Guo, J.; Dai, H. N-Doping of Graphene through Electrothermal Reactions with Ammonia. *Science* **2009**, *324*, 768−771.

(6) Gong, K.; Du, F.; Xia, Z.; Durstock, M.; Dai, L. Nitrogen-Doped Carbon Nanotube Arrays with High Electrocatalytic Activity for Oxygen Reduction. *Science* **2009**, *323*, 760−764.

(7) Tang, Y.; Allen, B. L.; Kauffman, D. R.; Star, A. Electrocatalytic Activity of Nitrogen-Doped Carbon Nanotube Cups. *J. Am. Chem. Soc.* **2009**, *131*, 13200−13201.

(8) Chang, D. W.; Lee, E. K.; Park, E. Y.; Yu, H.; Choi, H. J.; Jeon, I. Y.; Sohn, G. J.; Shin, D.; Park, N.; Oh, J. H.; et al. Nitrogen-Doped Graphene Nanoplatelets from Simple Solution Edge-Functionalization for n-Type Field-Effect Transistors. *J. Am. Chem. Soc.* **2013**, *135*, 8981−8988.

(9) Qu, L.; Liu, Y.; Baek, J.-B.; Dai, L. Nitrogen-Doped Graphene as Efficient Metal-Free Electrocatalyst for Oxygen Reduction in Fuel Cells. *ACS Nano* **2010**, *4*, 1321−1326.

(10) Kim, H.; Lee, K.; Woo, S. I.; Jung, Y. On the Mechanism of Enhanced Oxygen Reduction Reaction in Nitrogen-Doped Graphene Nanoribbons. *Phys. Chem. Chem. Phys.* **2011**, *13*, 17505−17510.

(11) Li, Y.; Zhao, Y.; Cheng, H.; Hu, Y.; Shi, G.; Dai, L.; Qu, L. Nitrogen-Doped Graphene Quantum Dots with Oxygen-Rich Functional Groups. *J. Am. Chem. Soc.* **2011**, *134*, 15−18.

(12) Rao, C. V.; Cabrera, C. R.; Ishikawa, Y. In Search of the Active Site in Nitrogen-Doped Carbon Nanotube Electrodes for the Oxygen Reduction Reaction. *J. Phys. Chem. Lett.* **2010**, *1*, 2622−2627.

(13) Kurak, K. A.; Anderson, A. B. Nitrogen-Treated Graphite and Oxygen Electroreduction on Pyridinic Edge Sites. *J. Phys. Chem. C* **2009**, *113*, 6730−6734.

(14) Li, Y.; Zhou, W.; Wang, H.; Xie, L.; Liang, Y.; Wei, F.; Idrobo, J. C.; Pennycook, S. J.; Dai, H. An Oxygen Reduction Electrocatalyst Based on Carbon Nanotube−Graphene Complexes. *Nat. Nanotechnol.* **2012**, *7*, 394−400.

(15) Chen, P.; Xiao, T. Y.; Qian, Y. H.; Li, S. S.; Yu, S. H. A Nitrogen-Doped Graphene/Carbon Nanotube Nanocomposite with Synergistically Enhanced Electrochemical Activity. *Adv. Mater.* **2013**, *25*, 3192−3196.

(16) Kosynkin, D. V.; Higginbotham, A. L.; Sinitskii, A.; Lomeda, J. R.; Dimiev, A.; Price, B. K.; Tour, J. M. Longitudinal Unzipping of Carbon Nanotubes To Form Graphene Nanoribbons. *Nature* **2009**, *458*, 872−876.

(17) Cruz-Silva, R.; Morelos-Gomez, A.; Vega-Diaz, S.; Tristan-Lopez, F.; Elias, A. L.; Perea-Lopez, N.; Muramatsu, H.; Hayashi, T.; Fujisawa, K.; Kim, Y. A.; et al. Formation of Nitrogen-Doped Graphene Nanoribbons via Chemical Unzipping. *ACS Nano* **2013**, *7*, 2192−2204.

(18) Allen, B. L.; Kichambare, P. D.; Star, A. Synthesis, Characterization, and Manipulation of Nitrogen-Doped Carbon Nanotube Cups. *ACS Nano* **2008**, *2*, 1914−1920.

DOI: 10.1021/acsami.5b00447
ACS Appl. Mater. Interfaces 2015, 7, 10734−10741

(19) Zhao, Y.; Tang, Y. F.; Chen, Y. A.; Star, A. Corking Carbon Nanotube Cups with Gold Nanoparticles. *ACS Nano* **2012**, *6*, 6912−6921.
(20) Zhao, Y.; Tang, Y.; Star, A. Synthesis and Functionalization of Nitrogen-Doped Carbon Nanotube Cups with Gold Nanoparticles as Cork Stoppers. *J. Visualized Exp.* **2013**, e50383.
(21) Li, Y.; Hu, Y.; Zhao, Y.; Shi, G.; Deng, L.; Hou, Y.; Qu, L. An Electrochemical Avenue to Green-Luminescent Graphene Quantum Dots as Potential Electron-Acceptors for Photovoltaics. *Adv. Mater.* **2011**, *23*, 776−780.
(22) Pan, D.; Zhang, J.; Li, Z.; Wu, M. Hydrothermal Route for Cutting Graphene Sheets into Blue-Luminescent Graphene Quantum Dots. *Adv. Mater.* **2010**, *22*, 734−738.
(23) Li, J. F.; Huang, Y. F.; Ding, Y.; Yang, Z. L.; Li, S. B.; Zhou, X. S.; Fan, F. R.; Zhang, W.; Zhou, Z. Y.; Wu, D. Y.; et al. Shell-Isolated Nanoparticle-Enhanced Raman Spectroscopy. *Nat. Nanotechnol.* **2010**, *464*, 392−395.
(24) Wustholz, K. L.; Henry, A.-I.; McMahon, J. M.; Freeman, R. G.; Valley, N.; Piotti, M. E.; Natan, M. J.; Schatz, G. C.; Duyne, R. P. V. Structure−Activity Relationships in Gold Nanoparticle Dimers and Trimers for Surface-Enhanced Raman Spectroscopy. *J. Am. Chem. Soc.* **2010**, *132*, 10903−10910.
(25) Lee, J.-H.; Nam, J.-M.; Jeon, K.-S.; Lim, D.-K.; Kim, H.; Kwon, S.; Lee, H.; Suh, Y. D. Tuning and Maximizing the Single-Molecule Surface-Enhanced Raman Scattering from DNA-Tethered Nanodumbbells. *ACS Nano* **2012**, *6*, 9574−9584.
(26) Zhou, X.; Huang, X.; Qi, X.; Wu, S.; Xue, C.; Boey, F. Y. C.; Yan, Q.; Chen, P.; Zhang, H. In Situ Synthesis of Metal Nanoparticles on Single-Layer Graphene Oxide and Reduced Graphene Oxide Surfaces. *J. Phys. Chem. C* **2009**, *113*, 10842−10846.
(27) Schedin, F.; Lidorikis, E.; Lombardo, A.; Kravets, V. G.; Geim, A. K.; Grigorenko, A. N.; Novoselov, K. S.; Ferrari, A. C. Surface-Enhanced Raman Spectroscopy of Graphene. *ACS Nano* **2010**, *4*, 5617−5626.
(28) Lv, R.; Li, Q.; Botello-Mendez, A. R.; Hayashi, T.; Wang, B.; Berkdemir, A.; Hao, Q.; Elias, A. L.; Cruz-Silva, R.; Gutierrez, H. R., et al. Nitrogen-Doped Graphene: Beyond Single Substitution and Enhanced Molecular Sensing. *Sci. Rep.* **2012**, *2*.
(29) Zhao, Y.; Burkert, S. C.; Tang, Y.; Sorescu, D. C.; Kapralov, A. A.; Shurin, G. V.; Shurin, M. R.; Kagan, V. E.; Star, A. Nano-Gold Corking and Enzymatic Uncorking of Carbon Nanotube Cups. *J. Am. Chem. Soc.* **2015**, *137*, 675−684.
(30) Higginbotham, A. L.; Kosynkin, D. V.; Sinitskii, A.; Sun, Z.; Tour, J. M. Lower-Defect Graphene Oxide Nanoribbons from Multiwalled Carbon Nanotubes. *ACS Nano* **2010**, *4*, 2059−2069.
(31) Tang, Y.; Allen, B. L.; Kauffman, D. R.; Star, A. Electrocatalytic Activity of Nitrogen-Doped Carbon Nanotube Cups. *J. Am. Chem. Soc.* **2009**, *131*, 13200−13201.
(32) Tang, Y.; Burkert, S. C.; Zhao, Y.; Saidi, W. A.; Star, A. The Effect of Metal Catalyst on the Electrocatalytic Activity of Nitrogen-Doped Carbon Nanotubes. *J. Phys. Chem. C* **2012**, *117*, 25213−25221.
(33) Sharifi, T.; Hu, G.; Jia, X.; Wagberg, T. Formation of Active Sites for Oxygen Reduction Reactions by Transformation of Nitrogen Functionalities in Nitrogen-Doped Carbon Nanotubes. *ACS Nano* **2012**, *6*, 8904−8912.
(34) Lai, L. F.; Potts, J. R.; Zhan, D.; Wang, L.; Poh, C. K.; Tang, C. H.; Gong, H.; Shen, Z. X.; Jianyi, L. Y.; Ruoff, R. S. Exploration of the Active Center Structure of Nitrogen-Doped Graphene-Based Catalysts for Oxygen Reduction Reaction. *Energy Environ. Sci.* **2012**, *5*, 7936−7942.
(35) Chu, H.; Zhang, J.; Liu, J.; Li, Y. Decoration of Gold Nanoparticles on Surface-Grown Single-Walled Carbon Nanotubes for Detection of Every Nanotube by Surface-Enhanced Raman Spectroscopy. *J. Am. Chem. Soc.* **2009**, *131*, 14310−14316.

DOI: 10.1021/acsami.5b00447
ACS Appl. Mater. Interfaces 2015, 7, 10734−10741